Hadronic Calorimetry for the ePIC Detector at the Electron–Ion Collider

The ePIC Collaboration

[Author list and affiliations to be inserted]

Working draft: September 16, 2026

Abstract

The asymmetric electron–ion collisions at the Electron–Ion Collider produce hadronic final states whose characteristic energy increases strongly from the electron-going to the hadron-going direction. Hadronic calorimetry in the ePIC detector is therefore implemented with three region-specific systems: the negative-pseudorapidity hadronic calorimeter (nHCal), a steel–scintillator tail catcher optimized for low-energy charged hadrons and neutrons; the barrel hadronic calorimeter (BHCal), based on the refurbished sPHENIX Outer HCal and serving simultaneously as the solenoid flux return; and the longitudinally segmented forward hadronic calorimeter (LFHCal), including a high-granularity insert around the beam pipe for energetic forward hadrons and jets. The systems use plastic scintillator and silicon-photomultiplier readout, CALOROC front-end electronics, LED and minimum-ionizing-particle calibration, and a common simulation and reconstruction environment, while differing in sampling fraction, depth, transverse segmentation, and longitudinal readout. The present design is supported by low-energy neutron and cluster-separation simulations for nHCal, operational and test-beam heritage together with ePIC full-detector simulations for BHCal, and prototype development and combined electromagnetic–hadronic performance simulations for LFHCal. These studies demonstrate the complementary roles of the three calorimeters in neutral-hadron reconstruction, muon identification, hadronic energy measurement, jet reconstruction, and particle-flow measurements. Experimental source-scan and beam-test results not documented in the preliminary design report remain to be incorporated in the final manuscript.

Contents

1 Introduction

1.1 Hadronic final states at the Electron–Ion Collider

The Electron–Ion Collider (EIC) will collide polarized electrons with polarized protons and light ions, and electrons with heavier ions, over a broad range of center-of-mass energies. The large asymmetry between the electron and hadron beam energies is directly reflected in the laboratory-frame final state. The electron-going, or backward, region is populated predominantly by relatively low-energy particles, while the hadron-going, or forward, region receives energetic hadrons and jets. Simulated 18×275 GeV electron–proton events contain forward single particles with energies as large as approximately 150 GeV, whereas the backward calorimeter is driven by the efficient detection of neutrons and charged hadrons at energies of order 1 GeV.

This rapidity dependence precludes a single optimal calorimeter geometry. At negative pseudorapidity, a high sampling fraction and a low threshold are more valuable than extreme depth. In the barrel, tracking and electromagnetic calorimetry measure most of the jet energy, and the hadronic calorimeter constrains the otherwise inaccessible neutral-hadron component while also providing robust minimum-ionizing-particle (MIP) identification. In the forward region, deteriorating track momentum and angular resolution, high particle energies, and nontrivial jet substructure require a deep calorimeter with fine transverse and longitudinal segmentation. These different conditions motivate the three-part ePIC hadronic calorimeter system.

1.2 Role of hadronic calorimetry in ePIC

The ePIC hadronic calorimeters measure neutral hadrons, sample the energy of charged hadrons after the electromagnetic calorimeters, and provide spatial information for calorimeter clustering and track–cluster association. Their principal system-level functions are:

- reconstruction and tagging of neutrons and other neutral hadrons;
- constraint of the jet-energy scale and jet-energy resolution;
- reconstruction of hadronic event kinematics and particle-flow objects;
- identification of charged-current deep-inelastic-scattering events through the hadronic final state and missing transverse energy;
- electron–hadron and muon–hadron discrimination using longitudinal response and MIP signatures; and
- neutral-energy tagging and vetoing in diffractive and jet measurements.

These functions are complementary to the high-precision charged-particle measurement provided by tracking and to the photon and electron measurement provided by electromagnetic calorimetry. In particular, hadronic calorimetry supplies the neutral component that cannot be recovered from charged-particle tracks.

1.3 Purpose and scope

This article presents the ePIC hadronic calorimetry as a single detector system. Its central design principle is the use of related steel–scintillator calorimetry and silicon-photomultiplier (SiPM) readout concepts, adapted to three distinct energy, occupancy, and containment regimes. The absorber depth, sampling fraction, transverse cell size, longitudinal segmentation, and signal grouping are optimized region by region, while the front-end ASIC, calibration concepts, simulation environment, and particle-flow principles are shared where practical. The emphasis is on the relationship between detector requirements, technology choices, validation, and expected performance. Detailed subsystem construction notes and individual test campaigns are intended to be reported separately.

2 System-Level Requirements and Detector Architecture

2.1 Coordinate system, acceptance, and detector interfaces

The ePIC coordinate system places the interaction point at the origin, with the positive z direction defined by the outgoing hadron beam and the negative z direction by the outgoing electron beam. Pseudorapidity is $\eta = -\ln\tan(\theta/2)$, where θ is measured with respect to positive z. The terms *forward* and *backward* therefore refer to positive and negative pseudorapidity, respectively.

The nHCal covers the backward acceptance $-4.14 < \eta < -1.18$ and is installed behind the backward electromagnetic calorimeter as a tail catcher. Its front face is at $z = -3.87$ m. The BHCal surrounds the central detector outside the solenoid and covers approximately $-1.1 < \eta < 1.1$; its steel absorber also provides the central solenoid flux return. The LFHCal begins at $z = 3.68$ m and covers $1.2 < \eta < 3.5$, while its beam-pipe insert extends the nominal acceptance to $3.5 < \eta < 4.4$. The forward electromagnetic calorimeter is mounted on the LFHCal front plate and contributes approximately one interaction length before the hadronic calorimeter. The numerical values in this article reproduce the preliminary design-report snapshot supplied for this draft and require a common configuration tag before publication.

Additional input needed: Provide a configuration-controlled ePIC longitudinal cross-section, geometry tag, and approval date. The hadronic-calorimeter source files do not contain a single figure showing all three systems and their interfaces.

2.2 Region-dependent particle environment and requirements

Table 1 summarizes the different optimization targets. For the nHCal, the most demanding quantitative requirement is greater than 90% detection efficiency for 1 GeV neutrons, accompanied by separation of clusters whose impact points are 30 cm apart and timing of order 200–300 ps for use in beam-background rejection. The BHCal requirement is approximately $50\%/\sqrt{E/\mathrm{GeV}} \oplus 10\%$ for standalone hadronic energy resolution, although its physics role is dominated by neutral-energy tagging in a particle-flow environment. The LFHCal is required to reconstruct hadrons within jets over approximately 5–250 GeV with fine spatial segmentation and sufficient depth for containment. Its combined forward electromagnetic–hadronic requirement is also $50\%/\sqrt{E/\mathrm{GeV}} \oplus 10\%$.

Radiation and rate environments also differ. The 15-year, 150 fb^{-1} 1-MeV-neutron-equivalent fluence is estimated below 10^{10} cm^{-2} over the nHCal and approximately $(5\text{–}7) \times 10^8$ cm^{-2} at the BHCal SiPM radius. In the LFHCal the annual fluence is strongly radius dependent, reaching approximately 10^{11} $\mathrm{cm}^{-2}\,\mathrm{yr}^{-1}$ nearest the beam pipe. This gradient motivates larger-area SiPMs and maintainable insert layers in the most exposed forward region.

2.3 Common performance definitions

For a calorimeter response distribution with mean reconstructed energy $\langle E_{\mathrm{reco}}\rangle$, the response and relative resolution are defined as $\langle E_{\mathrm{reco}}\rangle/E_{\mathrm{true}}$ and $\sigma(E_{\mathrm{reco}})/\langle E_{\mathrm{reco}}\rangle$, respectively. A conventional stochastic-plus-constant parameterization is

$$\frac{\sigma_E}{E} = \frac{a}{\sqrt{E/\mathrm{GeV}}} \oplus b, \tag{1}$$

Table 1: Principal requirements and design responses of the ePIC hadronic calorimeters. Values are taken from the preliminary design-report snapshot and remain subject to configuration control.

Requirement	Backward nHCal	Barrel BHCal	Forward LFHCal
Nominal acceptance	$-4.14 < \eta < -1.18$	approximately $\lvert\eta\rvert < 1.1$	$1.2 < \eta < 3.5$; insert to $\eta = 4.4$
Characteristic objects	Low-energy hadrons, neutrons, and MIPs	Neutral jet component and MIPs	High-energy hadrons and jets
Principal metric	Low threshold and detection efficiency	Neutral-energy constraint and muon identification	Energy and position resolution, containment, and shower separation
Depth strategy	Ten high-sampling-fraction steel–scintillator layers	Existing tilted steel flux-return structure, 3.8λ	Sixty layers, 5.8–6.5λ
Transverse segmentation	10×10 cm^2 baseline tiles	$\Delta\eta \times \Delta\phi \simeq 0.1 \times 0.02$	5×5 cm^2 cells; smaller hexagons in insert
Longitudinal information	Ten physical samples; final electronic grouping not specified	Multiple radial tile crossings	Seven readout segments; insert tiles individually read out
Validation emphasis	Low-energy shower simulation; optical validation input pending	sPHENIX heritage and ePIC geometry/reconstruction	Engineering prototypes and beam tests; detailed results pending

where a is the stochastic term, b is the constant term, and the terms are added in quadrature. The sampling fraction is the fraction of deposited energy recorded in active scintillator. Detection efficiency is the fraction of generated particles satisfying a stated reconstructed-energy or photoelectron threshold within a stated integration time. Linearity is assessed from the reconstructed response as a function of true energy. The ratio e/h denotes the relative electromagnetic and hadronic response of the sampling structure.

Position resolution and two-particle separation must be distinguished. The former is the width of the residual between reconstructed and true impact positions; the latter is the distance at which two showers satisfy a specified splitting efficiency or purity. MIP signal-to-noise is the most-probable MIP signal divided by the relevant electronic and photosensor noise measure. Leakage and containment refer to energy escaping the active calorimeter volume and the fraction retained within it. A final performance paper must state fit ranges, selection criteria, estimators, thresholds, integration windows, and the handling of non-Gaussian tails for every quoted result.

3 Common Detector, Readout, and Simulation Concepts

3.1 Plastic scintillator and photosensor readout

All three calorimeters use plastic scintillator read out by SiPMs, but the optical implementations reflect the available geometry and heritage. The nHCal and LFHCal use a direct SiPM-on-tile concept derived from CALICE developments [**?**, **?**]. A SiPM sits in a central dimple in the scintillator, and the tile is isolated with reflective foil. The nHCal baseline uses $10 \times 10 \times 2.4$ cm^3 tiles and Hamamatsu S14160-1315PS SiPMs. The larger nHCal transverse tile size can reduce response near tile edges, but the design study argues that the broad lateral extent of hadronic showers mitigates this loss at cluster level. Quantitative source-scan validation of that statement is not contained in the supplied report.

The main LFHCal uses $5 \times 5 \times 0.4$ cm^3 square tiles. Most tiles are planned to be injection molded at Fermilab because this route is at least an order of magnitude less expensive at full-detector scale, although their measured light yield is 20–25% lower than that of comparable cast sheet. Cast scintillator is reserved for the higher-radiation region below approximately 1 m radius where added light yield provides operational margin. The insert uses 3-mm-thick hexagonal cells, painted at their edges with TiO_2 and assembled in layer-specific frames. Candidate LFHCal SiPMs have active areas of 1.3×1.3 mm^2 in most regions and 3×3 mm^2 at radii below 1 m. Bench measurements reported for a 3×3 mm^2 S14160-3015PS coupled to an 8 cm^2 EJ-212 cell give a most-probable signal near 60 photoelectrons per MIP at approximately 2 V overvoltage [?].

The BHCal retains the sPHENIX optical system. Its 7-mm-thick extruded polystyrene tiles contain 1.5% PTP and 0.01% POPOP and have a chemically produced diffuse reflective coating. A 1-mm-diameter Kuraray Y11 wavelength-shifting fiber is embedded in each tile, routed so that deposited energy is within 2.5 cm of a fiber, and coupled at both polished ends to a 3×3 mm^2 SiPM. The existing photosensors will be replaced by Hamamatsu S14160-3015PS devices. Thus, the BHCal preserves a mature fiber-coupled architecture while the endcaps use direct SiPM-on-tile readout.

For all systems the operating gain varies with temperature and radiation history. Integrated LEDs and bias adjustment provide gain tracking, and the nHCal design explicitly includes distributed temperature sensors. SiPM saturation, optical cross-talk, dark-count contributions, photon-detection efficiency, and the temperature coefficient of gain must be included in the final digitization descriptions.

3.2 Absorber and sampling structures

Steel is the principal absorber in all three systems. The nHCal baseline alternates 4.0-cm steel plates with 2.4-cm scintillator. This comparatively large active-to-passive ratio is chosen because simulated low-energy neutron efficiency depends more strongly on the scintillator-to-absorber ratio than on the total layer count once more than approximately five layers are present. The ten-layer device is therefore a high-sampling-fraction tail catcher rather than a conventional deep energy-measuring calorimeter.

The BHCal uses tapered AISI-1020 low-carbon-steel plates tilted by 12° from the radial direction. The thickness increases from 26.1 mm at the inner radius to 42.4 mm at the outer radius, and a radial track traverses at least four scintillator tiles. The sampling fraction correspondingly decreases from 0.037 to 0.028. In addition to absorbing hadronic showers, this steel provides the central solenoid flux return, fixing the broad mechanical envelope and limiting the degree to which the sampling structure can be altered for ePIC.

The LFHCal alternates sixty 15.2-mm steel plates with sixty 4-mm scintillator layers. Its total depth is 5.8–6.5 interaction lengths depending on trajectory and module location. The approximately one interaction length supplied by the forward electromagnetic calorimeter is part of the combined forward response and must be treated explicitly in calibration. LFHCal module steel also contributes to the magnet flux return and is nickel plated after electron-beam welding to limit corrosion and wear.

3.3 Front-end electronics and streaming readout

The calorimeter systems use the self-triggered CALOROC ASIC, which supports the ePIC streaming-readout model. The design-report snapshot specifies 36 channels per ASIC, a 12-bit ADC for lower-amplitude signals, a 16-bit time-over-threshold path for larger signals, and channel-by-channel SiPM-bias trimming over 0–2.5 V. Charge injection provides a relative calibration of the ADC and time-over-threshold scales. The detailed timing transfer, absolute dynamic range, shaping settings, and zero-suppression configuration were not frozen in the supplied calorimeter sections.

The signal grouping differs by region. Every BHCal tile is read out independently in ePIC, replacing the sPHENIX scheme in which five SiPM signals were summed into one tower channel. The LFHCal transports analog signals passively to the module rear and sums corresponding tiles from 5–10 consecutive layers before digitization, producing seven longitudinal readout segments per 5×5 cm^2 tower. Insert cells are instead read out individually. The nHCal will use CALOROC boards on its front face, but the final layer grouping and resulting channel count are not specified.

Table 2: Readout parameters documented in the preliminary design report. A dash marks information that was not specified.

Parameter	nHCal	BHCal	LFHCal and insert
Photosensor	S14160-1315PS	S14160-3015PS	1.3- or 3-mm-class Hamamatsu SiPM
Signal grouping	–	one tile per channel	5–10 layers per sum; insert individual
Readout channels	–	7680	61,264 main + approximately 7000 insert
Longitudinal segments	–	tile-level radial sampling	7 main; 60 individual insert layers
ASIC	CALOROC	CALOROC	CALOROC
ADC / ToT	12 bit / 16 bit	12 bit / 16 bit	12 bit / 16 bit
Gain monitoring	LED and temperature	reused LED-fiber distribution	LED, charge injection, MIPs

Additional input needed: Freeze the CALOROC revision, shaping and timing settings, absolute charge ranges, sampling and streaming parameters, nHCal signal grouping, total nHCal channel count, and subsystem cable lengths.

3.4 Simulation, digitization, calibration, and reconstruction

The common reconstruction concept is

$$\begin{aligned} \text{energy deposition} &\longrightarrow \text{scintillation light} \longrightarrow \text{SiPM signal} \\ &\longrightarrow \text{digitized channel} \longrightarrow \text{calibrated cell} \longrightarrow \text{cluster and particle flow.} \end{aligned} \tag{2}$$

Detector geometry is implemented in the ePIC simulation environment and shower transport is performed with GEANT4. The active-energy deposits are converted to reconstructed cell energies through subsystem-specific sampling fractions and digitization. Cells are grouped with the standard island-clustering algorithm. Track–cluster matching identifies charged contributions, after which tracking momentum or the energy of an isolated charged cluster can be subtracted to estimate the neutral energy.

The available studies document several geometry snapshots but do not provide a single common software release. BHCal single-hadron response uses the 2024.10.1 simulation geometry, while its MIP and DIS tile-response studies use 2024.11.1. The nHCal studies use the official full ePIC simulation and EICrecon but do not state release tags in the calorimeter section. The LFHCal performance uses graph-neural-network (GNN) reconstruction following Ref. [?], but the source section does not state the common geometry, GEANT4 version, physics list, digitization, training/test partition, or uncertainty treatment. These omissions prevent a strict cross-subsystem comparison at present.

At hadronic scale, additional calibration is necessary because dead material, invisible nuclear energy, leakage, shower fluctuations, and clustering alter the response. For the BHCal, linear-discriminant and multilayer-perceptron regressions implemented with TMVA [**?**] combine the leading BHCal and barrel imaging calorimeter (BIC) clusters with energy sums from the BIC imaging and scintillating-fiber layers. For LFHCal, a graph network performs cell-level software compensation for the noncompensating steel–scintillator response, for which $e/h \simeq 1.2$. The nHCal neutral-energy studies instead use thresholded clusters and charged-energy subtraction.

Additional input needed: Provide one reproducible software table covering geometry tags, event generators, GEANT4 version and physics list, digitization, calibration constants, clustering parameters, reconstruction release, sample sizes, and systematic variations for every result retained in the article.

4 Region-Specific Calorimeter Designs

4.1 Backward hadronic calorimeter: nHCal

4.1.1 Physics requirements

The nHCal is a tail catcher in the electron-going direction. Its acceptance is motivated by low-Q^2, low-x processes, with particular sensitivity to $x \sim 10^{-3}$–10^{-2} and high inelasticity. Diffractive vector-meson and dijet topologies can place low-energy neutral and charged particles at backward rapidity. The calorimeter therefore provides a neutral-energy veto and improves scattered-electron identification in conjunction with the backward electromagnetic calorimeter. The design target is greater than 90% efficiency for 1 GeV neutrons and three-standard-deviation separation of clusters 30 cm apart. MIP sensitivity is required for muon/pion discrimination, with a target pion rejection of order 10^2 at greater than 90% muon efficiency. Timing of order 200–300 ps is intended to aid rejection of hadron-beam backgrounds together with the LFHCal.

4.1.2 Geometry and module concept

The baseline nHCal is a flattened annular cylinder with outer radius 2.76 m and inner radius 0.14 m. The front face is at $z = -3.87$ m. Ten layers of 4.0-cm steel alternate with 2.4-cm plastic-scintillator tiles, giving 64 cm of calorimeter depth and reserving 9 cm of the available 75-cm envelope for readout electronics. The first active layer faces the interaction point, improving sensitivity to low-momentum charged particles, MIPs, background vetoes, and the start of neutral showers.

The 10×10 cm^2 tiles use direct SiPM-on-tile readout. Tile and absorber layers are assembled into $10 \times 20 \times 64$ cm^3 modules patterned after the LFHCal construction. The source states that 294 modules are foreseen, each containing twenty scintillator tiles and ten absorber plates. CALOROC electronics are located on the front face and services enter through the gap between the backward endcap elements. The support and cooling design depends on the final channel granularity.

4.1.3 Design optimization

Single-particle simulations scanned the number of layers and the ratio of scintillator to absorber thickness. For 0.9-GeV neutrons, the active-to-passive ratio has a larger effect on detection efficiency than the total number of layers; beyond approximately five layers, adding layers produces little further efficiency gain in the reported scan. Threshold and integration time remain important at the lowest energies. At a threshold of $0.1E_{\text{MIP}}$ and a 100-ns integration window, the simulation gives greater than 70% efficiency for 300-MeV neutrons. Separate tile-size studies quantify cluster efficiency and position resolution.

These studies motivate a high sampling fraction and low threshold, but they do not constitute a complete multi-objective optimization. The preliminary design report does not provide mass and cost curves, a quantitative MIP signal-to-noise study, SiPM-saturation margins, e/h and linearity versus geometry, or a documented comparison of tile surface treatments. It also does not show that the stated 2.4-cm scintillator thickness is selected by a validated optical model.

Additional input needed: Supply the nHCal baseline version and decision record, including the full thickness scan, optical coupling and surface-treatment variants, mass and cost, MIP signal-to-noise, dynamic range, SiPM saturation, fabrication constraints, and robustness to threshold and integration-window uncertainties.

4.2 Barrel hadronic calorimeter: BHCal

4.2.1 Reuse of the sPHENIX Outer HCal

The BHCal is based on the sPHENIX Outer HCal, a mature steel–scintillator sampling calorimeter developed through simulation, prototype, and beam-test studies. Thirty-two azimuthal sectors contain tilted tapered steel plates interleaved with scintillator tiles. The envelope spans radii from approximately 1.82 to 2.70 m and a length of 6.316 m. The absorber tilt ensures that a radial track crosses at least four tiles. The total depth is approximately 3.8λ, and the same steel returns the central-solenoid magnetic flux.

The standalone single-particle resolution measured for the sPHENIX design is reported as $75\%/\sqrt{E/\text{GeV}} \oplus 14.5\%$. A final article should cite the original beam-test publication and reproduce its particle selection, fit range, leakage configuration, and uncertainty before using this value as a direct validation of ePIC performance.

4.2.2 Modifications for ePIC

The principal ePIC modification is the transition from tower-summed to tile-level readout. In sPHENIX the analog signals from five SiPMs are combined into one tower channel. In ePIC each of the 7680 tiles is read independently with a new S14160-3015PS SiPM and CALOROC channel. The resulting nominal segmentation is $\Delta\eta \times \Delta\phi \simeq 0.1 \times 0.02$, based on 24 tile bins in pseudorapidity and 320 in azimuth. This factor-of-five increase in electronic segmentation preserves the mechanical sampling but exposes the radial hit pattern for clustering and MIP identification.

The existing LED fiber-distribution network will be reused. Each half-sector contains five bundles of 25 fibers, of which 24 illuminate tiles and one is spare. Three chimney sectors must be recut to accommodate the larger ePIC solenoid-service chimney, removing the shortened tiles in the affected region. All sector SiPMs will be replaced, cables and electronics will be installed, and every tile will be checked before integration.

4.2.3 Reconstruction consequences

Individual-tile readout permits clustering directly from tile cells instead of pre-summed towers. It improves sensitivity to the multi-layer MIP signature and provides additional information for splitting and merging hadronic showers. Hadron calibration must combine the BHCal with the BIC because particles lose energy in upstream material and because the BIC contains both scintillating-fiber and imaging layers. The demonstrated regression inputs include leading BHCal and BIC cluster energies and the summed energy in six AstroPix and twelve scintillating-fiber BIC layers.

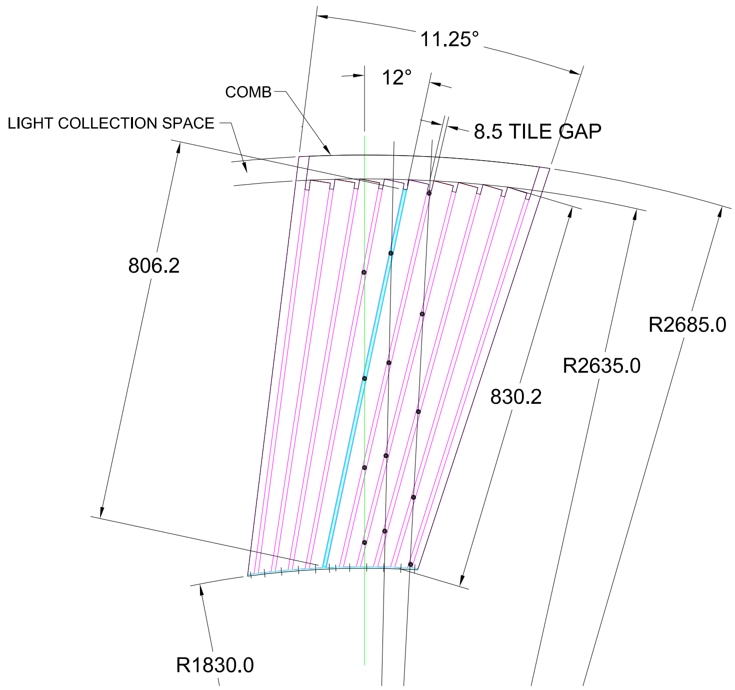

Figure 1: Transverse cutaway of an sPHENIX Outer HCal sector, the basis of the ePIC BHCal. Tapered absorber plates are tilted relative to the radial direction, while scintillator tiles and their light-collection services occupy the gaps. Dimensions are those of the preliminary design-report snapshot.

The full-detector neutron samples show pronounced low-energy tails even after regression calibration. The source attributes these provisionally to cluster splitting, hadronic-shower fluctuations, or model inadequacy. These effects, along with dead material and low-energy neutron transport, must be understood before a precision neutral-hadron resolution is quoted.

4.3 Longitudinal forward hadronic calorimeter: LFHCal and insert

4.3.1 Forward physics requirements

The forward calorimeters intercept the highest-energy particles in the central detector. PYTHIA simulations of 18×275 GeV electron–proton collisions give single-particle energies up to approximately 150 GeV, and typical radius-$R = 1$ jets contain 10–12 particles with measurable substructure. Tracking momentum and angular resolution worsen rapidly beyond $\eta \simeq 3$, so calorimetry must provide both energy measurement and shower position. Fine segmentation and small inactive regions are also important for particle-flow association and two-particle separation.

4.3.2 Mechanical and sampling design

The LFHCal has an outer radius of approximately 2.7 m and total mechanical depth of 1.32 m. Sixty 15.2-mm steel plates alternate with sixty 4-mm scintillator layers. The main detector contains 1058 eight-tile (8M) modules and 72 four-tile (4M) modules in the design table, although a later paragraph in the source quotes 1052 8M modules and the total stack count elsewhere is also inconsistent. This discrepancy must be resolved by configuration control.

Each 8M active layer comprises eight approximately 4.7×4.7 cm^2 tiles on a flexible SiPM carrier, giving a nominal 5×5 cm^2 cell pitch. Sixty such layers slide into an electron-beam-welded, nickel-plated AISI-1020 steel structure. A long passive transfer board carries the analog signals to the rear, where summing and CALOROC digitization are accessible. Groups of 5–10 layers form seven longitudinal readout segments per tower. The main LFHCal contains 8752 towers and 61,264 readout channels.

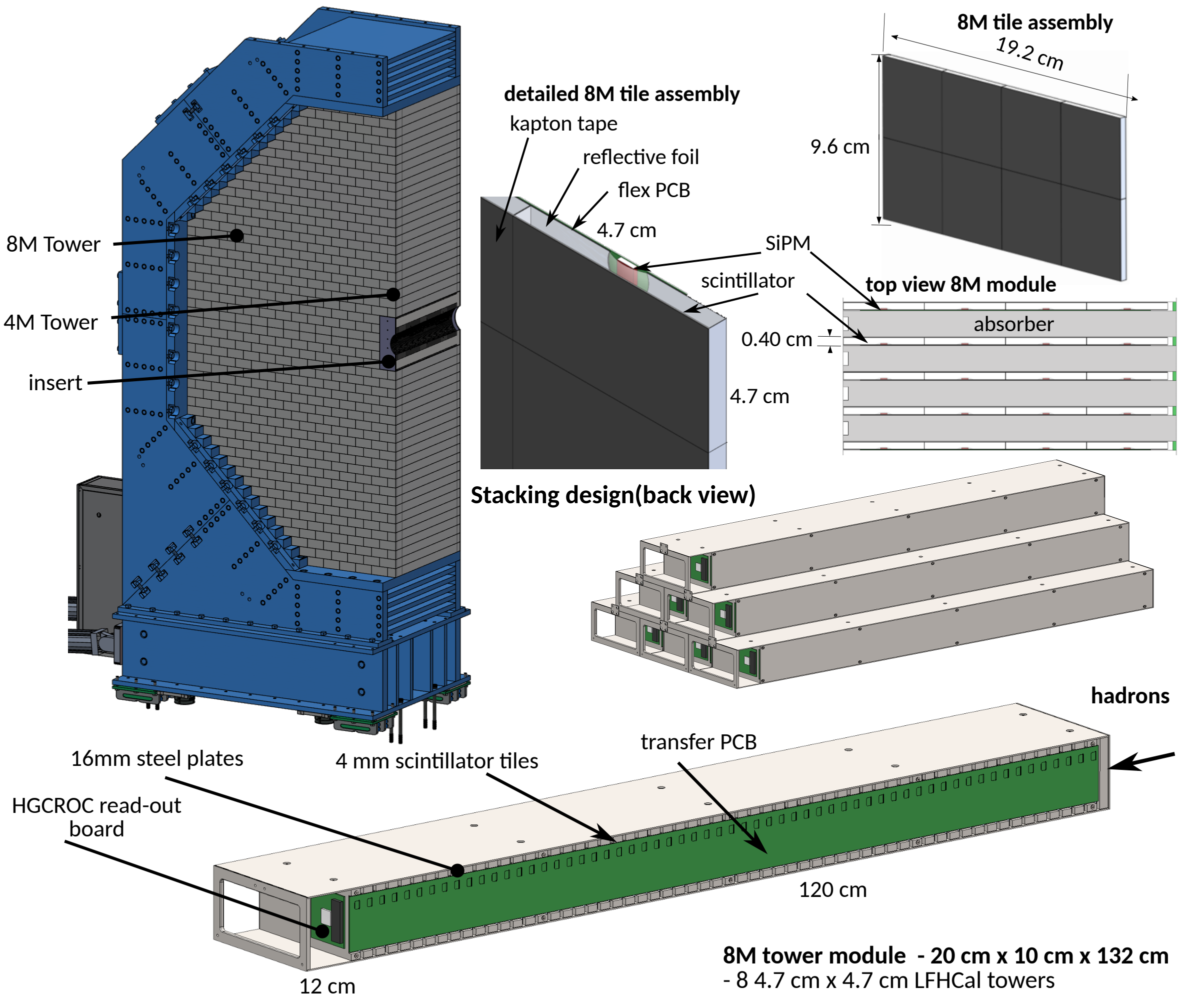

Figure 2: LFHCal design overview showing the calorimeter half, square-tile SiPM-on-tile assembly, layer stack, and 8M module. The graphic predates the final CALOROC labeling; dimensions and component names should be updated to the publication baseline.

The complete detector is stacked as two movable half-discs on rail-mounted cradles. Modules are positioned with shims, fixed at the rear, and bolted to a 25.4-mm front plate that also supports the forward electromagnetic calorimeter. Approximately 1000 readout ASICs, dissipating an estimated 2 W each, are distributed over the rear face and cooled by a small liquid system.

4.3.3 High-granularity forward insert

Two insert modules surround the conical beam-pipe aperture. They cover approximately $3.5 < \eta < 4.4$ and are designed for removal during extended shutdowns so that radiation-damaged SiPMs can be replaced or annealed. The first twenty layers use staggered hexagonal cells approximately 4.2 cm wide; the remaining forty layers use approximately 6.5-cm cells. The four-layer staggering pattern provides overlapping spatial samples that can be exploited by subcell algorithms such as HEXPLIT or by machine-learning reconstruction [**?**, **?**].

Unlike the main LFHCal, every insert tile is read out individually to preserve position information and enable cell-by-cell monitoring in the strongly nonuniform radiation field. Approximately 7000 insert channels are anticipated. The source is internally inconsistent about the exact number of insert SiPMs required for procurement, so a frozen channel map is needed.

5 Experimental Validation Program

5.1 nHCal validation

The preliminary design report documents simulation of neutron efficiency, threshold, integration time, sampling ratio, tile-size scaling, and two-particle separation. It also specifies module-level QA with LED illumination, optical-isolation tests, and cosmic-ray alignment. It does not document the large-tile radioactive-source scans or the associated optical simulation called for by the manuscript outline.

Additional input needed: Provide the nHCal tile sample matrix, scintillator manufacturer and surface finish, thicknesses, dimple and optical coupling, wrapping, SiPM model and operating point, ^{90}Sr apparatus, trigger and scan geometry, environmental conditions, raw-to-photoelectron calibration, uncertainties, optical-photon simulation, residual maps, and quantitative goodness of fit. Clarify whether the scanned tiles are production-like.

5.2 BHCal validation

The BHCal validation chain begins with the established sPHENIX Outer HCal design and its prototype beam tests, followed by construction experience and operation in Au+Au and proton–proton collisions. The source reports that leakage-current evolution in sPHENIX remains below operational limits and that the substantially lower ePIC fluence should provide additional margin. The mechanical design, tile optical chain, cosmic calibration, and LED distribution are therefore supported by direct detector experience.

For ePIC, the full detector geometry has been exercised with MIPs, charged pions, neutrons, and deep-inelastic-scattering events. The tile-level simulation produces a clear reconstructed MIP peak near 250 MeV for 2–20 GeV muons within $|\eta| < 1$, well above the anticipated cell threshold. Full-detector pion and neutron studies demonstrate the need for combined BIC–BHCal calibration and expose low-energy tails and cluster splitting. These results validate the reconstruction pathway but do not replace a hardware demonstration of the new photosensor, longer cable, CALOROC, and individual-tile configuration.

The existing sPHENIX HCal prototype is planned for a dedicated test of individual-tile rather than tower-summed readout. Sector refurbishment will additionally be validated through electrical checks and cosmic-ray measurements after SiPM replacement. Three test stands at BNL, Georgia State University, and the University of New Hampshire are being prepared for this program.

Additional input needed: Add the original sPHENIX beam-test citation and data, the ePIC individual-tile prototype configuration and results, cable-noise measurements, MIP efficiency and purity, calibration-transfer uncertainty, and a direct tower-summed versus tile-level comparison.

5.3 LFHCal validation

The design report states that partial or single-module campaigns were completed in 2023 and 2024, and that campaigns with progressively larger prototypes are planned over 2025–2028. It further reports that first summing-board and long-transfer-board prototypes were received and tested in 2025. The detector design and production approach have therefore progressed beyond component drawings, but the supplied calorimeter section contains no beam species, energies, event selections, calibration procedures, response plots, or data–simulation comparisons.

Additional input needed: For each main-LFHCal and insert campaign, provide the dates and facility, prototype depth, absorber and scintillator configuration, instrumented layers, tile production route, wrapping, SiPM and bias, transfer/summing boards, front-end electronics, beam species and energies, trigger and event selection, MIP calibration, stability, linearity, resolution, longitudinal profiles, saturation, dynamic range, GEANT4 comparison, uncertainties, and manufacturing lessons.

6 Simulation-Based Subsystem Performance

6.1 Common single-particle response presentation

The current simulation results establish subsystem feasibility but were produced with different geometry snapshots, particle samples, calibrations, and estimators. A publication-quality comparison should regenerate charged-pion, neutron, proton, and muon samples in a common release, using shared energy points and pseudorapidity bins. For each particle the presentation should include efficiency, mean response, linearity, resolution, non-Gaussian tails, longitudinal leakage, and position response. Thresholds and integration windows must be included in the nHCal efficiency definition, while forward and barrel results must distinguish standalone HCal response from combined electromagnetic–hadronic response.

Additional input needed: A common single-particle production is not included in the preliminary design report. We want consistent response plots for each system.

6.2 Backward performance

The simulated optimization shows that low-energy neutron detection is governed primarily by sampling fraction. For 0.9-GeV neutrons, increasing the scintillator-to-absorber ratio produces a larger efficiency change than adding sampling layers, and the reported efficiency saturates above approximately five layers. At the chosen low threshold of $0.1E_{\mathrm{MIP}}$ and a 100-ns integration window, the efficiency exceeds 70% at 300 MeV. These results support the use of thick scintillator and a low-noise readout, but the final 1-GeV efficiency at the stated baseline and its systematic uncertainty must still be tabulated against the greater-than-90% requirement.

The tile-size scan and two-particle samples address spatial performance. In simulated 1-GeV neutron–pion pairs, the showers can be distinguished at impact-point separations near 30 cm. Neutral-energy reconstruction begins to degrade at 33.9 cm, is strongly affected below 25.6 cm, and becomes effectively ambiguous below 8.7 cm. In a diffractive-dijet sample, 0.7% of projected neutron–other-particle pairs are separated by less than 30 cm. At reconstructed-cluster level, merging is visible below 20 cm; 22% of truth neutron–other clusters but only 5% of reconstructed pairs lie within 30 cm, demonstrating the selection effect introduced by merging.

For jets, a full ePIC simulation study reports an approximately 20% improvement in the resolution of a charged-only jet selection when nHCal information is used to veto jets with neutral

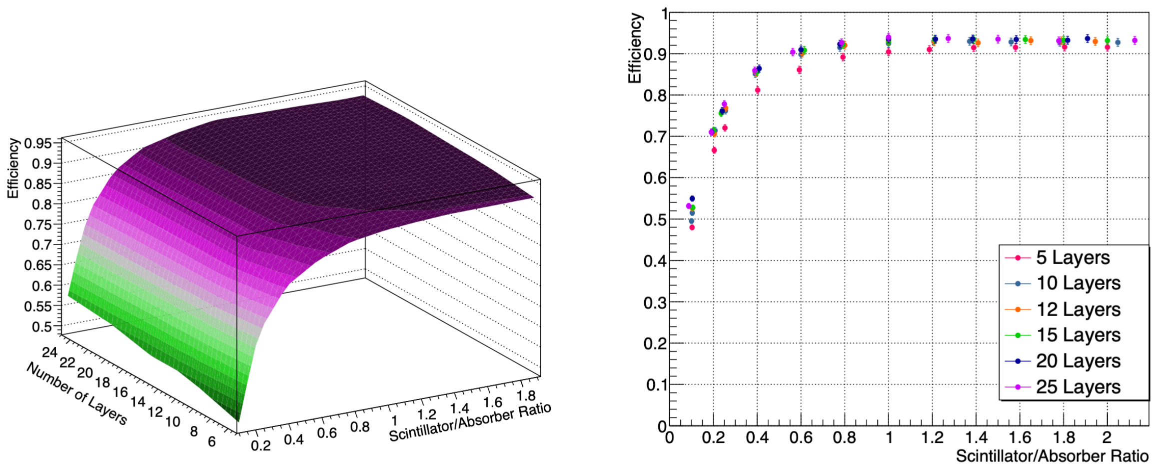

Figure 3: Simulated 0.9-GeV neutron efficiency as a function of the number of sampling layers and the scintillator-to-absorber thickness ratio. The final manuscript must add the geometry tag, threshold, integration window, event count, and uncertainty definition.

hadrons. The study uses MC-assisted matching and should therefore be interpreted as a potential performance bound rather than a fully data-driven particle-flow result.

The outline anticipates a validation chain

$$\begin{aligned}\text{source-scan data} &\longrightarrow \text{validated optical model} \longrightarrow \text{photoelectron threshold model}\\ &\longrightarrow \text{full-shower simulation} \longrightarrow \text{low-energy efficiency and baseline thickness.}\end{aligned} \tag{3}$$

Only the full-shower portion of Eq. (3) is documented in the supplied report. The source scan cannot by itself select the calorimeter sampling thickness; it must first constrain light collection and threshold response, which are then propagated into the full detector optimization.

6.3 Barrel performance

Single muons simulated with energies from 2 to 20 GeV and $|\eta| < 1$ produce a distinct reconstructed tile-energy peak near 250 MeV. This confirms that tile-level readout can expose a MIP signature, but the efficiency and purity of a complete muon tag have not yet been quantified.

BHCal-only simulations of 2–20 GeV charged pions produce recognizable leading-cluster peaks after correction to the electromagnetic scale. In the full detector these peaks broaden because of upstream energy loss, invisible energy, shower fluctuations, and clustering inefficiency. Linear-discriminant and multilayer-perceptron regressions combining BHCal and BIC information restore a more nearly Gaussian charged-pion response. The source reports that the calibrated resolution satisfies the design requirement, while noting a pathology for the 20-GeV negative-pion MLP result. The same calibration applied to neutrons improves the mean response, but substantial low-energy tails remain.

Fast-simulation studies cited in the source show the role of the neutral component in barrel jets and hadronic event kinematics, including Jacquet–Blondel reconstruction and missing transverse energy. Because some of these plots use an ECCE detector parameterization or Yellow Report Delphes studies rather than the present ePIC geometry, they are not treated here as final BHCal performance.

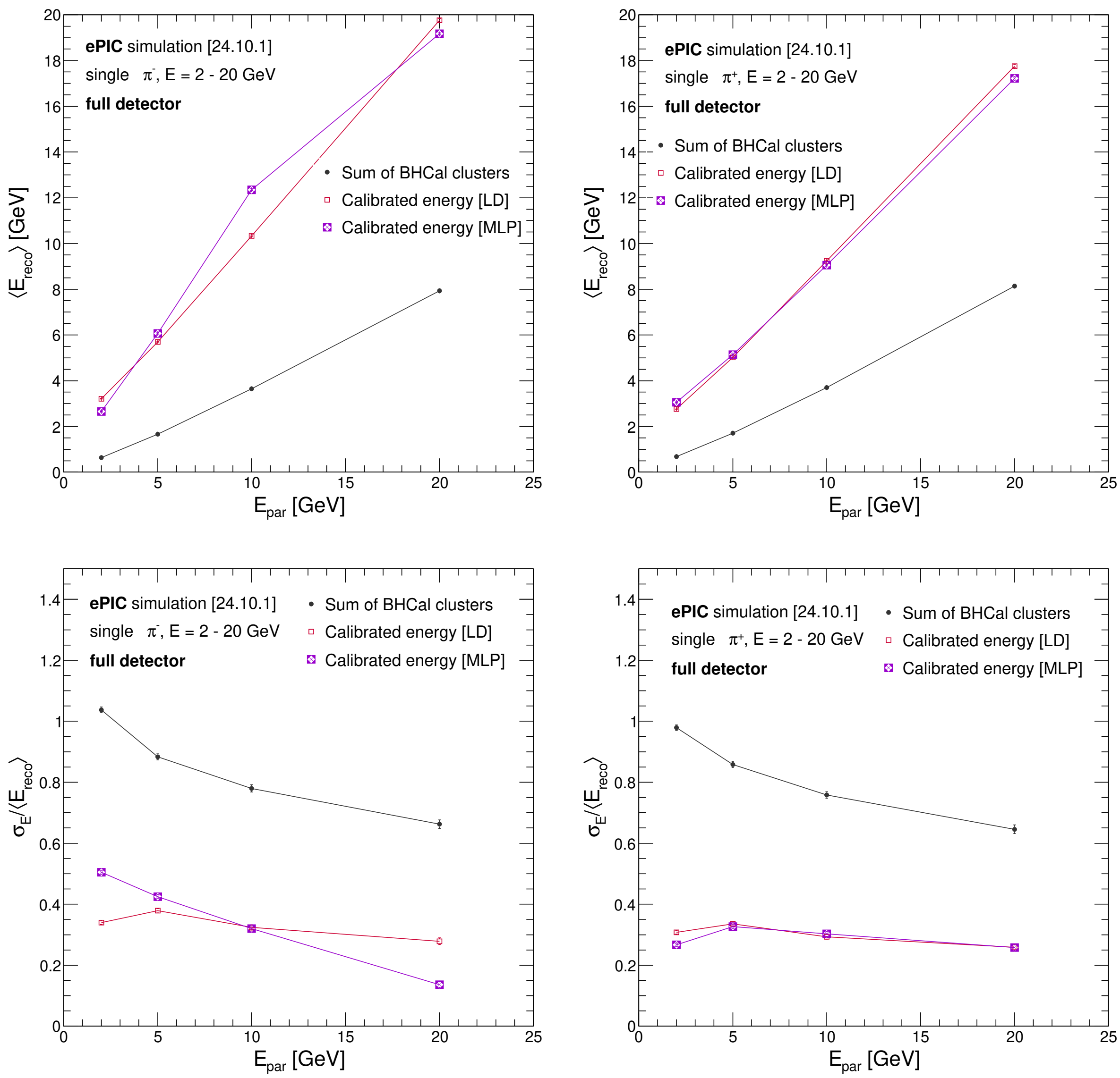

Figure 4: Linearity (top) and relative energy resolution (bottom) for calibrated single negative pions (left) and positive pions (right) in the 2024.10.1 ePIC geometry. The curves compare linear-discriminant and multilayer-perceptron calibrations with an uncalibrated BHCal cluster sum. Training and test statistics and systematic uncertainties must be added.

Additional input needed: Provide an ePIC tile-versus-tower comparison, quantitative MIP-tag efficiency and purity, final charged-pion and neutron fit values with uncertainties, a validated treatment of neutron tails and dead material, and current ePIC jet-energy scale and resolution.

6.4 Forward performance

The steel–scintillator LFHCal is noncompensating, with a simulated $e/h \simeq 1.2$. The forward electromagnetic calorimeter adds approximately one interaction length and has a different response, so energy reconstruction is performed jointly. A GNN uses cell-level shower information to implement event-by-event software compensation and to reduce sensitivity to fluctuations in the electromagnetic shower fraction [**?**, **?**].

For single pions in the principal LFHCal acceptance, the preliminary study reports a combined forward electromagnetic–hadronic resolution of

$$\frac{\sigma_E}{E} = \frac{27\%}{\sqrt{E/\mathrm{GeV}}} \oplus 3\%, \tag{4}$$

which is better than the stated $50\%/\sqrt{E/\mathrm{GeV}} \oplus 10\%$ requirement. The combined azimuthal and polar-angle resolutions are better than 4 mrad for pion energies above 5 GeV throughout the studied acceptance. The polar-angle resolution improves mildly with energy to approximately 2.5 mrad, while the azimuthal resolution improves with increasing pseudorapidity to below approximately 2.5 mrad.

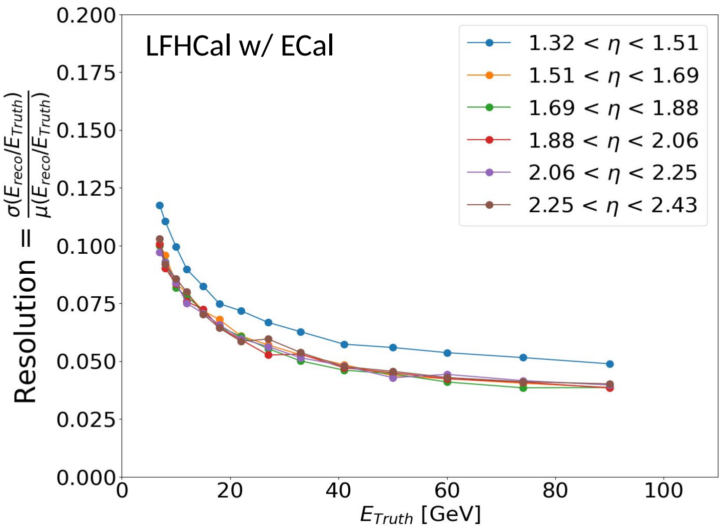

Figure 5: Combined forward electromagnetic–hadronic energy resolution for single pions as a function of true energy in pseudorapidity intervals, obtained with GNN reconstruction. The plot covers the primary LFHCal acceptance shown in the source study.

The result demonstrates the value of longitudinal and transverse shower information, but the report does not provide separate leakage and dead-region corrections, two-particle separation, insert-only response, jet performance, or systematic uncertainties. The quoted resolution also applies to a combined calorimeter and GNN chain, not to the standalone LFHCal.

Additional input needed: Provide response linearity, leakage and containment, dead-region corrections, conventional-reconstruction and ablation baselines for the GNN, training details and uncertainties, two-particle separation, insert-only performance, and particle-flow and jet results.

7 Combined ePIC Performance and Detector Interfaces

7.1 Transition regions

The nominal acceptances leave the nHCal–BHCal and BHCal–LFHCal transition regions near $\eta \simeq -1.1$ and $\eta \simeq 1.1$–1.2, respectively. The calorimeter sections describe local envelopes but do not provide a continuous material map or common response scan through these boundaries. Services, the solenoid, electromagnetic calorimeters, endcap support plates, and cracks can alter shower development and clustering in precisely these regions.

Additional input needed: Provide the frozen material and acceptance map and a common single-particle or physics-event sample versus pseudorapidity, including cracks, support, services, thresholds, cluster migration, and uncertainty bands at both transitions.

7.2 MIP Detection

Additional input needed: Primarily focus on muons in HCALs, provide rapidity coverage plots for e.g. VM->mu+mu-, "identification", meaning the pi rejection factor, the effective efficiency given energy loss

7.3 Electromagnetic–hadronic calorimeter matching

All three systems depend on their adjacent electromagnetic calorimeter. The nHCal catches leakage from the backward electromagnetic calorimeter and supplies a hadronic tag for scattered-electron identification. In the barrel, BIC layer and cluster energies enter the hadronic-scale regression together with BHCal clusters. In the forward region, the electromagnetic and hadronic calorimeters are calibrated as a combined system because the electromagnetic calorimeter itself contributes approximately one interaction length and the two systems have different e/h values.

At reconstruction level, spatial association must connect calorimeter clusters to extrapolated tracks. Charged-energy subtraction then uses the more precise track momentum when appropriate, leaving a neutral-energy estimate. The nHCal two-particle study implements an example of this logic: either the pion momentum or the reconstructed charged-cluster energy is subtracted from the total, depending on consistency between charged-cluster energy and momentum. A unified ePIC algorithm will additionally require timing matching, leakage recovery, intercalibration, and treatment of clusters shared across subsystem boundaries.

Additional input needed: Document the common track-propagation and matching windows, timing criteria, E/p consistency test, leakage recovery, charged-energy subtraction, ambiguity resolution, and electromagnetic–hadronic calibration.

7.4 Particle-flow and jet reconstruction

The hardware segmentation is chosen to support particle flow: tracking measures charged particles, electromagnetic calorimetry measures photons and electrons, and hadronic calorimetry supplies neutral hadrons and shower leakage. The nHCal study demonstrates improved charged-only jet selection after vetoing jets with neutral activity. The BHCal design exposes individual tiles to aid neutral-cluster separation and MIP tagging. The LFHCal supplies 5×5 cm^2 cells and seven depth segments, while its insert provides individual hexagonal cells in the region where tracking is least constraining.

No single study in the supplied material compares tracking-only, calorimetry-only, and combined particle-flow jets in the current full ePIC geometry. Some barrel figures originate from earlier ECCE or Delphes parameterizations and should serve only as motivation.

Additional input needed: Provide a controlled ePIC comparison using a stated jet algorithm and radius, particle-level reference, energy and pseudorapidity bins, matching criteria, calibration and corrections, neutral fraction, fake and inefficiency rates, and systematic uncertainty.

7.5 Common calibration and monitoring

The calibration hierarchy begins with electronic charge injection and SiPM gain monitoring, proceeds through cell or tile intercalibration, and ends with electromagnetic-to-hadronic scale corrections from physics events and simulation. All systems use LED light injection. The LFHCal explicitly includes charge injection for relative ADC/ToT calibration; the nHCal design explicitly includes temperature sensors to track SiPM gain, while the BHCal will reuse its mature LED-fiber distribution and sPHENIX calibration experience.

MIPs provide an in-situ reference. LFHCal tower sums will be monitored with collision tracks and cosmic muons, nHCal will use physics events and cosmics for monitoring and alignment, and every refurbished BHCal sector will receive a cosmic-ray calibration. In sPHENIX, the HCal electromagnetic scale was established by matching cosmic-muon ADC distributions to realistic simulation, supplemented by azimuthal symmetrization in collision data and temperature corrections. ePIC plans to adapt this strategy, with isolated tracks and momentum balance providing additional hadronic-scale constraints.

Additional input needed: Freeze the calibration cadence, reference observables, channel acceptance criteria, temperature coefficients, LED stability requirements, database and versioning model, time-alignment procedure, and in-situ samples for absolute scale and long-term monitoring.

8 Engineering, Production, and Quality Assurance

The construction programs reflect the distinct maturity of the three systems. The nHCal shares module and SiPM-on-tile technology with LFHCal. Its 294 modules are planned to contain ten electron-beam-welded absorber plates and twenty scintillator tiles each. Module QA will use the calibration system to verify tile response, photosensor connection, and optical isolation, but detailed acceptance thresholds remain to be defined.

The BHCal program is a controlled refurbishment. After sPHENIX disassembly, sectors will be inspected, SiPMs replaced, cables installed, and every tile read out with dedicated electronics. Cosmic data will determine relative tile calibration. Three chimney sectors require machining for the ePIC service aperture. Twenty-nine regular sectors can retain their installed tiles. Spare production is estimated at 470 replacement tiles, with greater numbers for the two innermost shapes.

LFHCal production is the largest effort. Electron-beam-welded absorber structures receive dimensional inspection and nickel plating. The preliminary QA plan calls for full geometricdimensioning-and-tolerancing inspection of 5% of regular modules, external-dimension and go/no-go slot checks for the remainder, and full inspection of insert modules. Random samples of each SiPM batch will be checked for breakdown voltage, gain dependence, and noise. Every scintillator assembly will receive visual light-tightness inspection, dimensional checks, connectivity tests, and single-photoelectron measurements under a traceable identifier. Transfer boards will be tested for continuity and cross-talk, front-end cards for function, and completed modules with electrical tests and cosmic rays.

Approximately 90% of main-LFHCal tiles are expected to be injection molded and 10–12% machined from cast sheet. More than 525,000 square tiles are required by the quoted production plan, making automated reflective-foil cutting and wrapping important for schedule and dimensional control. Insert layers are individually assembled from edge-painted hexagonal cells and removable carrier structures. Module weights range from approximately 74 kg to 1.3 t, requiring engineered lifting fixtures, controlled storage, and assembly procedures.

Common production principles should include component serialization, dimensional and optical acceptance criteria, SiPM batch traceability, light-tightness, electronics burn-in, calibration constants linked to geometry versions, and documented handling of nonconformances. Installation surveys and service verification must be repeated after the movable endcap cradles return to the beam position.

Additional input needed: Provide approved production baselines and schedules, quantitative QA acceptance limits, cooling and service margins, installation tolerances, readiness milestones, and the resolution of inconsistent LFHCal module counts.

9 Conclusions

The ePIC hadronic-calorimeter system uses three implementations because the laboratory-frame hadronic final state changes markedly with pseudorapidity. The backward nHCal prioritizes low threshold and sampling fraction for low-energy neutrons and MIPs; the BHCal exploits a mature tilted steel–scintillator flux-return structure to measure neutral barrel energy and tag MIPs; and the LFHCal supplies the depth and three-dimensional segmentation required for energetic forward hadrons and jets.

Plastic scintillator, SiPM readout, CALOROC electronics, LED monitoring, MIP calibration, GEANT4-based simulation, calorimeter clustering, and track–cluster association provide a common technical foundation. Risk is further reduced by nHCal/LFHCal technology sharing and by reuse of the operational sPHENIX Outer HCal. Experimental validation is currently strongest for the BHCal heritage and for component-level LFHCal development. The source-scan data anticipated for nHCal and the detailed LFHCal beam-test record were not present in the supplied preliminary design report and must be added before submission.

Simulation supports the central design choices. The nHCal studies demonstrate the importance of active-to-passive ratio, low threshold, and approximately 30-cm shower separation. Full-detector BHCal studies demonstrate MIP sensitivity and the need for combined BIC–BHCal hadronic calibration, while identifying unresolved neutron tails. A GNN applied to the combined forward calorimeters yields a reported single-pion resolution of $27\%/\sqrt{E/\mathrm{GeV}} \oplus 3\%$ and angular resolution better than 4 mrad above 5 GeV.

Several items remain under optimization or configuration control: nHCal optical and thickness validation, nHCal channel grouping, BHCal individual-tile hardware tests, LFHCal insert mapping and module counts, common software and reconstruction versions, transition-region response, and full ePIC particle-flow jet performance. Resolving these items will complete the link from component validation through subsystem response to the combined physics performance of ePIC.

A Proposed Figure and Table Inventory

The following items are recommended for the collaboration review draft. Items already represented by preliminary figures in this manuscript are marked “draft”; the remainder require new or approved material.

1. ePIC longitudinal cross-section with all hadronic calorimeters and interfaces – input needed.
2. Regional requirements and design-parameter comparison table – draft included.
3. Common signal, simulation, digitization, and reconstruction chain – equation included; graphic input needed.
4. nHCal baseline geometry and module concept – approved CAD input needed.
5. nHCal tile-sample table and ^{90}Sr apparatus – input needed.
6. nHCal data, optical simulation, residual map, and scan profiles – input needed.
7. nHCal thickness/performance optimization summary – simulation draft included.
8. BHCal geometry, refurbishment, and tile-readout modification – geometry draft included.
9. BHCal validation and tile-level reconstruction impact – hardware comparison input needed.
10. LFHCal and insert geometry, modules, and longitudinal grouping – draft included.
11. LFHCal prototype/beam-test data compared with simulation – input needed.
12. Common single-particle response and resolution summary – common production needed.
13. Combined particle-flow or jet-performance comparison – input needed.
14. Performance versus pseudorapidity, including transition regions – input needed.
15. Production and QA workflow or subsystem readiness table – approval needed.

B Information to Freeze Before Submission

- Geometry version, thicknesses, layer counts, depths, segmentation, channel counts, and acceptance for all subsystems.
- Resolution of the LFHCal 8M-module-count and insert-channel-count inconsistencies.
- Production-like status of nHCal tiles used for the principal optical result.
- Quantitative nHCal data–simulation agreement, residuals, uncertainties, and goodness-of-fit metric.
- Separation of optical-model validation from full-shower thickness optimization.
- Software release, geometry tag, GEANT4 version, physics list, digitization, reconstruction, and calibration versions for every simulation result.
- Beam-test configurations, beam conditions, selections, calibration procedures, data–simulation comparisons, and systematic uncertainties.
- Fit definitions and uncertainty treatment for all quoted resolution and efficiency values.
- Frozen versus provisional statements and an approval date for each design table.

- Scope boundaries and cross-references to detailed nHCal, BHCal, LFHCal, electronics, and test-beam publications.

Acknowledgments

Additional input needed: Insert the collaboration-approved funding, facility, technical-staff, and computing acknowledgments.

References